Received: 01 July 2016 | Accepted: 28 October 2016

DOI: 10.1111/gbi.12220

ORIGINAL ARTICLE

WILEY gebiology

Evidence of molybdenum association with particulate organic matter under sulfidic conditions

T. W. Dahl[1]* | A. Chappaz[2] | J. Hoek[1†] | C. J. McKenzie[3] | S. Svane[3] | D. E. Canfield[1]

[1]Nordic Center for Earth Evolution and University of Southern Denmark, Odense M, Denmark

[2]Department of Earth and Atmospheric Sciences, Central Michigan University, Mount Pleasant, MI, USA

[3]Department of Physics, Chemistry and Pharmacy, University of Southern Denmark, Odense M, Denmark

Correspondence
T. W. Dahl, Natural History Museum of Denmark, Copenhagen K, Denmark.
Email: tais.dahl@snm.ku.dk

Current address
*T. W. Dahl, Natural History Museum of Denmark, University of Copenhagen, Copenhagen K, Denmark.
Email: tais.dahl@snm.ku.dk

[†]Department of Geology, University of Maryland, College Park, MA, USA

Funding information
Nordic Center for Earth Evolution (NordCEE) of the Danish National Research Foundation, Grant/Award Number: DNRF53; VILLUM Foundation, Grant/Award Number: 1168439 and VKR023127; ACS-PRF, Grant/Award Number: 54583-DNI2; NSF-EAR, Grant/Award Number: 1503596

Abstract

The geochemical behavior of molybdenum (Mo) in the oceans is closely linked to the presence of sulfide species in anoxic environments, where Fe availability may play a key role in the Mo scavenging. Here, we show that Mo(VI) is reduced in the presence of particulate organic matter (represented by sulfate-reducing bacteria). Molybdenum was immobilized at the surface of both living cells and dead/lysed cells, but not in cell-free control experiments. Experiments were carried out at four different Mo concentrations (0.1 to 2 mM) to yield cell-associated Mo precipitates with little or no Fe, consisting of mainly Mo(IV)-sulfide compounds with molecular structures similar to Mo enzymes and to those found in natural euxinic sediments. Therefore, we propose that Mo removal in natural sulfidic waters can proceed via a non-Fe-assisted pathway that requires particulate organic matter (dead or living sulfate-reducing bacteria). This pathway has implications for global marine Mo cycling and the current use of Mo-based proxies for paleo-environmental investigations.

1 | INTRODUCTION

Molybdenum (Mo) is an essential trace metal in many metabolic pathways and has consequently played a key role in biospheric evolution (Anbar & Knoll, 2002). Like iron, it is an essential micronutrient for nearly all organisms, as it is required by enzymes catalyzing key reactions in global carbon, sulfur and nitrogen metabolism (Mendel & Bittner, 2006). This capacity makes Mo an important element in biology despite its scarcity in the Earth's crust (Taylor & Mclennan, 1995).

Modern and ancient sediments deposited beneath anoxic and sulfidic (euxinic) waters are typically enriched in Mo by up to two orders of magnitude relative to upper crustal material (1–2 μg/g) (Taylor & Mclennan, 1995) and organic-rich sediments deposited beneath oxic waters (~5 μg/g) (Dahl, Ruhl et al., 2013; Scott & Lyons, 2012). Given this contrasting, redox-dependent relationship, many studies have incorporated Mo as a proxy for the amount of oxygen in ancient and recent marine systems (Arnold, Anbar, Barling, & Lyons, 2004; Dahl, Hammarlund et al., 2010; Scott et al., 2008; Siebert, Nägler, Von Blanckenburg, & Kramers, 2003; Wille et al., 2007).

Molybdenum removal from the water column in the oceans is closely linked to the presence and accumulation of sulfide (total sulfide = ΣS(-II) = [H_2S + HS^- + S^{2-}]). With increasing ΣS(-II) concentration, molybdate (MoO_4^{2-}) is progressively transformed into thiomolybdate species ($MoO_{4-x}S_x^{2-}$) (Erickson & Helz, 2000). The following step responsible for Mo burial is a matter of debate. Previous studies demonstrated that Mo is removed from euxinic waters via adsorption on sinking particles, although Mo removal below sediment–water interface also occurs (Algeo & Tribovillard, 2009; Crusius,

Calvert, Pedersen, & Sage, 1996; Dahl, Anbar et al., 2010; Nameroff, Balistrieri, & Murray, 2002). Linear correlations between Mo and organic matter are observed in euxinic sediments and may suggest an organic Mo shuttle from the water column to the sediments (Lyons, Anbar, Severmann, Scott, & Gill, 2009). Yet, the mechanisms involved are not well understood, and the role of organic matter remains undefined.

Previously, Mo enrichments in sulfidic settings were thought to be attributed to molybdenite, MoS_2, precipitation (e.g., Amrhein, Mosher, & Brown, 1993; Biswas, Woodards, Xu, & Barton, 2009). However, it has been demonstrated that molybdenite does not form in aquatic systems under sulfidic conditions (Chappaz, Gobeil, & Tessier, 2008), and molybdenite present in some Ordovician black shales arguably formed via thermal maturation (Ardakani, Chappaz, Sanei, & Mayer, 2016). Otherwise, Mo can be found as distinct Mo(IV)-sulfide compounds in unknown, submicron, dispersed forms in anoxic muds and black shales (Bostick, Fendorf, & Helz, 2003; Dahl, Chappaz, Fitts, & Lyons, 2013; Helz et al., 1996). Among the potential pathways that could contribute to Mo enrichments in euxinic settings (e.g., Chappaz et al., 2014), two have received the most attention: the Fe pathway and the organic matter (OM) pathway.

In the Fe pathway, thiomolybdates can be reduced in the presence of zero-valent sulfur to create Mo-polysulfide species (Vorlicek, Kahn, Kasuya, & Helz, 2004) that are, for example, adsorbed or co-precipitated with FeS_2, FeS (Bostick et al., 2003; Freund et al., 2016; Helz, Vorlicek, & Kahn, 2004; Xu, Christodoulatos, & Braida, 2006), and clay minerals (i.e., illite and Fe-contaminated kaolinite and montmorillonite) (Bertine, 1972; Helz et al., 2004; Vorlicek & Helz, 2002). Some of these minerals may even be imbedded in an organic matrix in a coupled Fe-organic matter pathway (Dahl, Chappaz et al., 2013; Freund et al., 2016).

Based on these observations, Mo precipitation in euxinic systems has been recently discussed in the context of iron sulfide formation (Helz, Bura-Nakić, Mikac, & Ciglenečki, 2011). For example, Helz et al. (2011) proposed a specific pathway where thiomolybdate species react with FeS to form (e.g., nanoscale) FeMo sulfide minerals with the approximate formula, $FeMo_{0.6}S_{2.8}$ that precipitate in euxinic settings. Alternatively, Fe-Mo-S cuboidal clusters have been suggested as an important host phase for Mo in euxinic sediments (Dahl, Chappaz et al., 2013; Helz, Erickson, & Vorlicek, 2014; Helz et al., 1996). Previous Mo EXAFS characterizations of black shales have suggested Fe was present at ~2.6 Å from the average Mo atom (Helz et al., 1996), but the data quality of such natural samples displays high background/signal ratio at high k ($Å^{-1}$) values that significantly limits the determination of which atoms are present beyond the first shell of (mainly sulfur) ligands (discussed further below). The Mo-Fe-S hypothesis as formulated by Helz et al. (2011) implies that Mo removal in euxinic waters is FeS-limited and that Fe availability in sulfidic systems should affect sedimentary Mo enrichments (Tribovillard et al., 2015) and, perhaps even, impact the global marine molybdenum cycle.

The OM pathway is supported by observations that Mo concentrations in euxinic marine sediments (and even in some reducing sediments, where sulfide only accumulates at depth inside the sediments) invariably show strong, positive correlations with total organic carbon contents (TOC) (Algeo & Lyons, 2006; Poulson Brucker, Mcmanus, Severmann, & Berelson, 2009). Implicitly, these empirical Mo–TOC relationships have encouraged the view that OM can serve as a carrier of Mo from the sulfidic water column to the underlying sediments. Moreover, Mo is found disseminated within the matrix in euxinic sedimentary rocks, rather than concentrated in >10 μm pyrite grains (Chappaz et al., 2014; Tribovillard, Riboulleau, Lyons, & Baudin, 2004), supporting the idea of an interaction between Mo and OM during deposition (Dahl, Anbar et al., 2010; Glass et al., 2013). Further, we note that ~50% of the Mo found in the sulfidic part of the water column in Lake Cadagno is captured on 0.7 μm filter, suggesting Mo is adsorbed onto suspended particulates (Dahl, Anbar et al., 2010). Few studies, however, have provided mechanistic details on how Mo would be associated with particulate OM in sulfidic marine settings. One possibility might be Mo assimilation by nitrogen fixing bacteria. However, diazotrophs are insufficient in abundance and their Mo/C ratio is too low to produce high sedimentary Mo enrichments (e.g., Tuit, Waterbury, & Ravizza, 2004).

Experiments with living sulfate-reducing bacteria (SRB) grown at sublethal Mo levels (MoO_4^{2-} inhibits sulfate reduction at high concentrations) showed interactions between Mo and cell surfaces under sulfidic conditions (Biswas et al., 2009; Tucker, Barton, & Thomson, 1998a,b). Results from previous experiments suggest that: (i) Mo is enzymatically reduced in living cultures grown at 0.1–2.0 mM MoO_4^{2-} levels, (ii) reduction immobilizes Mo in the periplasm of the cell and (iii) the Mo precipitate is molybdenite, MoS_2, similar in form to the Mo observed in certain Mo ore deposits (i.e., rocks with ~10,000 ppm Mo), yet, imbedded in an organic matrix (Biswas et al., 2009). These observations suggest that particulate OM, and sulfate-reducing bacteria in particular, could play an important role in Mo scavenging processes. One limitation of previous studies, however, is that the concentration of Fe was not investigated, so an iron-assisted Mo removal pathway could not be ruled out. Secondly, previous studies lack appropriate kill control experiments to entirely exclude a potential non-living process. Lastly, the precipitates in previous experiments were characterized only indirectly by visual inspection and may not even contain MoS_2, and so, may well have another chemical form (Dahl, Chappaz et al., 2013).

The objectives of this study were as follows: (i) to test experimentally a possible interaction between Mo and particulate OM (represented by dead SRB), independent of Fe, in aqueous sulfidic solutions; (ii) to determine Mo speciation when adsorbed on particulate OM; and (iii) to discuss implications for the marine Mo cycle and paleoenvironmental reconstructions.

2 | MATERIALS AND METHODS

2.1 | Bacterial culture experiments

Experiments with pure cultures of *D. vulgaris Hildenborough* were prepared from stock cultures maintained in anaerobic salt-water carbonate buffered medium with lactate (10 mM) as the electron donor and primary carbon source. The medium composition was as follows: NaCl

(20 g/L), $MgCl_2{\cdot}6H_2O$ (3 g/L), Na_2SO_4 (4 g/L) [final concentration of sulfate = 28 mM], $CaCl_2{\cdot}2H_2O$ (0.15 g/L), NH_4Cl (0.25 g/L), KH_2PO_4 (0.2 g/L), KCl (0.5 g/L), and vitamins and trace metals (Widdel & Bak, 1992) containing Fe (26 μM) and Mo (0.38 μM). Few droplets of resazurin dye that turns purple in the presence of O_2 were added to the medium as an oxidation indicator. Medium was prepared after solutions were degassed with O_2-free N_2:CO_2 (90:10), and pH was adjusted to 7 using HCl. Ten ml of medium was anoxically transferred to Hungate tubes, sealed with butyl rubber stoppers, and transferred in an anaerobic chamber (COY, USA) under an atmosphere of N_2:H_2 (95%:5%).

Experiments were carried out in duplicate with dead cells (D), living cells (L), and cell-free controls (N) to assess whether Mo precipitation occurred with/without OM (D and L vs. N), and to test whether living cells actively trigger Mo precipitation (L vs. D). A sulfide-free, cell-free experiment (O) with medium and no cells but containing Mo was prepared to test the role of sulfide for Mo precipitation (N vs. O). Before Mo injection, D cultures were pre-grown and heat-killed by autoclave (121°C), whereas cultures for N experiments were pre-grown and filtered anaerobically. A fresh starter culture was also pre-grown and injected by syringe to L experiments. Molybdate (MoO_4^{2-}) was added simultaneously at the beginning of experiments L, D, N and O at the following concentrations: 0.1, 0.5, 1 and 2 mM. Cells were harvested at four different time intervals when L cultures were in the stationary and death phase (7, 12, 18, 24 and 42 days, Table S1). The cultures were killed in two distinct ways by sacrificing two tubes at the time of harvesting. In one replicate, cells were killed by first adding 0.5 ml 2 M NaOH to convert ΣS(-II) to S^{2-}, and then adding 1.0 ml poisonous Zn-acetate to fix S^{2-} as ZnS. Samples were shaken to a well-mixed slurry and ΣS(-II) concentrations were quantified on an aliquot of the slurry using the Cline method (Cline, 1969). In a second replicate, cells were killed quickly by the addition of 1 ml glutaraldehyde (4%) to each tube at the end of the experiment. Glutaraldehyde is an efficient cross-linking agent used for protein fixation (and immobilization of enzymes) (Migneault, Dartiguenave, Bertrand, & Waldron, 2004). Therefore, glutaraldehyde should not affect Mo speciation or Mo precipitation yield during the experiments. Indeed, Mo precipitation yields were similar or higher in cultures killed with glutaraldehyde compared to the NaOH-killed replicates. In all cases, cells were separated from supernatant by centrifugation (3220 *g*, 20 min) and filtration (0.45-μm membrane filter) inside an anaerobic chamber, and then solutes and precipitates were immediately frozen at −80°C. Samples were stored frozen and thawed in an anoxic (N_2:H_2 = 95%:5%) atmosphere before analyses.

Bacterial growth (cell density) was monitored by optical absorbance measurements at 595 nm using a UV-VIS spectrophotometer. As in previous experiments (Biswas et al., 2009), the presence of Mo limited growth in our culture experiments (Figure S1). In L experiments and D+N start-up cultures, $Na_2S{\cdot}9H_2O$ was injected to an initial ΣS(-II) level of 0.32 mM to ensure molybdate conversion to thiomolybdate would start immediately at the beginning of the experiment. For cell-free (N) and heat-killed (D) control experiments, start-up cultures were first grown under ideal conditions to achieve final sulfide concentrations well above the threshold for thiomolybdates formation in the media. As expected, ΣS(-II) levels remained high (1–13 mM) in L, D, and N experiments (Figure S2). Thiomolybdate concentrations were monitored by optical absorbance measurements using a UV-VIS spectrophotometer (Erickson & Helz, 2000). At the Mo/sulfide ratios used in our experiments, thermodynamic calculations predict that predominant species are $MoOS_3^{2-}$ and MoS_4^{2-}. As expected, all solutions were orange indicative of tri- and tetrathiomolybdate with characteristic absorption peaks at 318 nm and 468 nm, respectively.

2.2 | Synthesis of the $[Ph_4P]_2[Mo^V_2S_8]$

This known Mo^V-S compound (Pan, Harmer, Halbert, & Stiefel, 1984) was synthesized using a new method, in which internal electron transfer from S^{-II} to Mo^{VI} is induced upon reaction with an external one-electron oxidant Ce^{IV} (Pan et al., 1984). Here, $[NH_4]_2Ce[NO_3]_6$ (210 mg, 0.383 mmol) was added to a solution of $[NH_4]_2[MoS_4]$ (100 mg, 0.385 mmol) dissolved in dimethylformamide (5 ml) and was heated for 1 h at ca. 90°C after which $[Ph_4P]Br$ (300 mg, 0.716 mmol) was added. The solution was filtered hot to remove the small amount of solids. Diethylether:isopropanol (4:1) (25 ml) was added to the filtrate causing immediate precipitation of a black microcrystalline solid. This solid was collected and air-dried. The yield was 98 mg, corresponding to 45% yield. IR spectroscopy (Hitachi 270-30 IR spectrometer, KBr pellet) bands for the synthesized product ($[Ph_4P]_2[Mo^V_2S_8]$) are at 3,426, 3,051, 1,664, 1,584, 1,482, 1,435, 1,384, 1,186, 1,107, 996, 753, 722, 688, and 527 cm^{-1}. Powder X-Ray diffractograms (Rigaku Miniflex 600) could not be obtained due to the small amount of material synthesized, but the identity of the starting material $(NH_4)_2MoS_4$ was verified from patterns calculated from published single crystal X-Ray data (2θ range = 5–70°) (Lapasset, Chezau, & Belougne, 1976).

2.3 | Atomic Absorption Spectroscopic (AAS) analyses

Dissolved Mo concentrations were determined using a Perkin Elmer AAS-100 with a flame fueled by a mixture of acetylene and nitrous oxide. An aliquot of the solution (~2.2 ml of 10.5 ml) was first thawed and then diluted (at least 1:3) in 2% NH_4Cl run solution. Mo absorption was detected at 313.3 nm and converted to concentrations by interpolation via a six-point calibration curve.

2.4 | Inductively coupled plasma mass spectrometer (ICP-MS) analyses

Microbial precipitates (centrifugates, ~0.1 ml) were brought in solution in acid-cleaned Teflon beakers after a treatment with ~5 ml boiling, concentrated HNO_3 for 5 days. At the end, all digestions produced clear solutions. Mo and Fe concentrations were determined in this solution, at two separate dilutions (1:500 and 1:5), by Thermo Scientific X-Series ICP-MS. The intensity signal was calibrated by comparison with a five-point multi-element calibration curve. All solutions were analyzed in Ir-doped 2% HNO_3 to correct for plasma suppression in sample solutions (up to 20% decline of the Ir signal during the run).

2.5 | X-Ray Absorption spectroscopy (XAFS) analyses

To characterize Mo oxidation state and the molecular environment in the microbial precipitates, XAFS analyses were performed at beamlines X11-A and 13-BM-D at the National Synchrotron Light Source (Brookhaven National Laboratory) and Advanced Photon Source (Argonne National Laboratory), respectively. The procedure used is described in more detail in a previous study (Dahl, Chappaz et al., 2013). Briefly, absorption spectra were collected from −200 to +800 eV about the Mo-K-edge (~20,000 V) using a Si(311) or a Si(111) double crystal monochromator with an unfocused beam. Sample fluorescence was measured with a Canberra multichannel 13-element Ge detector. Four spectra were collected for each sample and averaged for analysis. There were no systematic temporal changes indicative of sample damage caused by the beam or photo-reduction between consecutive spectral measurements. Signal analysis of the X-ray absorption near edge structure (XANES) spectrum was performed in Matlab and distinctive features (K-edge energy and maximum absorption peak) plotted to estimate average Mo oxidation state and Mo-O vs. Mo-S coordination environments (Figure 1; Dahl , Chappaz et al., 2013).

The raw data were processed and analyzed using the Athena and Artemis software packages. The Extended X-Ray Absorption Fine Structure (EXAFS) fitting exercise requires both that the EXAFS equation can be established with physically reasonable parameter values (including total amplitude of photon energy, coordination number, distance to neighboring atoms, and Debye–Waller factors) and that the presented Mo structures fulfill the bond valence model described by Brown and Altermatt (1985) and Altermatt and Brown (1985). That is, the sum of the bond valence, $V = \sum_i \exp(R-R_i)/B$, is approximately equal to the formal oxidation state of the metal. Here, R and B are known constants (Table S2) (Brown & Altermatt, 1985), and R_i is bond length of the ith ligand. Model structures were only accepted if V was within ±0.3 units of the average oxidation state determined by XANES (as do our reference materials, Table S2). This approach allowed us to estimate the average bond lengths and coordination number of neighboring atoms (O vs. S) in the samples. However, EXAFS analysis of an unknown, complex material is not exact because the EXAFS equation is fit only to a single (dominant) Mo coordination geometry with no ability to cope with multiple scattering paths or multiple Mo phases present in each sample. Therefore, we assumed that our samples contain only Mo compounds with known coordination environments and searched for the best fit to Mo structures among well-characterized Mo enzymes and 110 relevant abiotic Mo(IV)-S and Mo(V)-S structures found in the Cambridge Structural Database (Table S2) (Allen, 2002).

3 | RESULTS AND DISCUSSION

3.1 | Sulfate-reducing bacteria grown at near-lethal Mo levels

Previous experiments with cultures of *D. desulfuricans*, *D. gigas*, and *D. vulgaris* Hildenborough (Biswas et al., 2009) showed how SRB grown at 0.1–2.0 mM molybdate concentration precipitated Mo in the periplasm of the cells. Here, we confirm that sulfidic cultures of *D. vulgaris* Hildenborough remove molybdate from the solution. Previous experimental studies found that *D. desulfuricans*, *D. gigas*, and *D. vulgaris* Hildenborough tolerated up to ~2 mM Mo, with *D. vulgaris* Hildenborough more sensitive to Mo than the others (Biswas et al., 2009). In our experiments, only two of eight replicate *D. vulgaris* Hildenborough experiments (4 time steps ×2 kill mechanisms) grew at ~0.5 mM molybdate (Table S1). No growth was observed in L cultures with ≥1.0 mM molybdate. This result was confirmed with all time replicates of the Mo-rich cultures by continuously monitoring the inactivity until day 42. The difference from the earlier study is perhaps explained by their better-adapted starting cultures. Molybdate concentrations in our culture experiments were dictated by the requirements for XAFS analysis as we wanted to obtain molecular information about a potential Mo—particulate OM interaction. Although Mo concentrations used in our study are 10^3- to 10^6-fold higher than

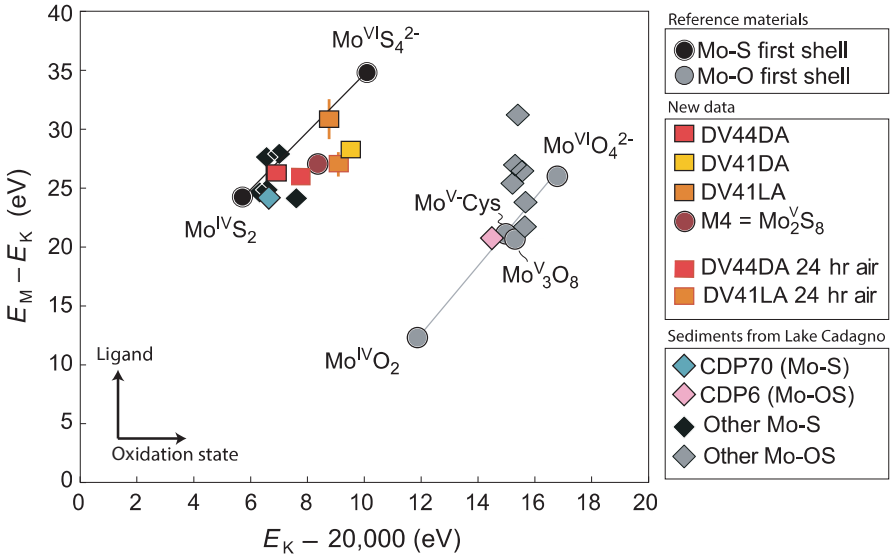

FIGURE 1 XANES spectroscopy allows for characterization of Mo oxidation state and distinction of Mo-O versus Mo-S compounds. A new Mo(V)-sulfide reference material, $[Ph_4P]_2Mo_2S_8$, shows that K-edge scale with Mo oxidation state. This improves accuracy of oxidation state determination of Mo-S compounds. Peaks and edges in the XANES spectra were identified using Matlab (details in caption to Figure S4) [Colour figure can be viewed at wileyonlinelibrary.com]

in natural sulfidic environments, our results suggest that Mo removal in our experiments could follow a similar chemical pathway in natural aquatic systems (we discuss this further below).

3.2 | Mo reduction with dead cells

In the presence of sulfide and in the absence of cells (N), $Mo^{VI}O_4^{2-}$ is progressively transformed into $Mo^{VI}O_{4-x}S_x^{2-}$ with characteristic orange colors (see example in Figure S3) detected at distinctive wavelengths (Erickson & Helz, 2000). For our conditions of pH (7) and sulfide concentration (ΣS(-II) >2 mM), we calculated the characteristic timescale of tri- and tetrathiomolybdate formation to be 0.5 and 48 hr, respectively (Erickson & Helz, 2000). As expected, we observed mostly tetrathiomolybdate in the L, D, and N solutions after >7 days, and never in sulfide-free control experiments (O). Previous workers attributed the orange color to the presence of Mo(IV) or Mo(V) species in the cultures (Biswas et al., 2009; Chen, Ford, & Clayton, 1998). However, it should be noted that the colors observed in our experiments match that of molybdate reacting with hydrogen sulfide (Erickson & Helz, 2000) to form $Mo^{VI}OS_3^{2-}$ and $Mo^{VI}S_4^{2-}$ in aqueous solution. Thus, considering only the orange color is not evidence for Mo reduction.

Molybdenum precipitates in sulfidic aqueous media both with heat-killed cells and live cultures of *D. vulgaris* Hildenborough (Figure 2). Dark precipitates were visible in dead cell control (D) experiments with 1–2 mM Mo. No precipitates were observed in sulfide-free controls (O), or in any of the cell-free experiments with sulfide (N) (Figure S3, Table S1). Molybdenum precipitation occurred predominantly within the first 7 days during the growth and stationary phase, but the precipitates were first harvested after 42 days during the death phase (Table S1). Average precipitation yields calculated from the supernatants at all time steps show that ~40% of the Mo in the live cultures and 20% to 75% in the dead cultures had precipitated after >7 days (Figure 2, Table S1). Measurements of Mo in the centrifugates show that a portion of Mo was lost upon filtration of the centrifuged solutions, which could be expected by Mo loss on smaller particulates (e.g., lysed cell material). In any case, this does not affect conclusions made in this study, where the objective is solely to document direct Mo—particulate OM interaction and to characterize the associated Mo speciation.

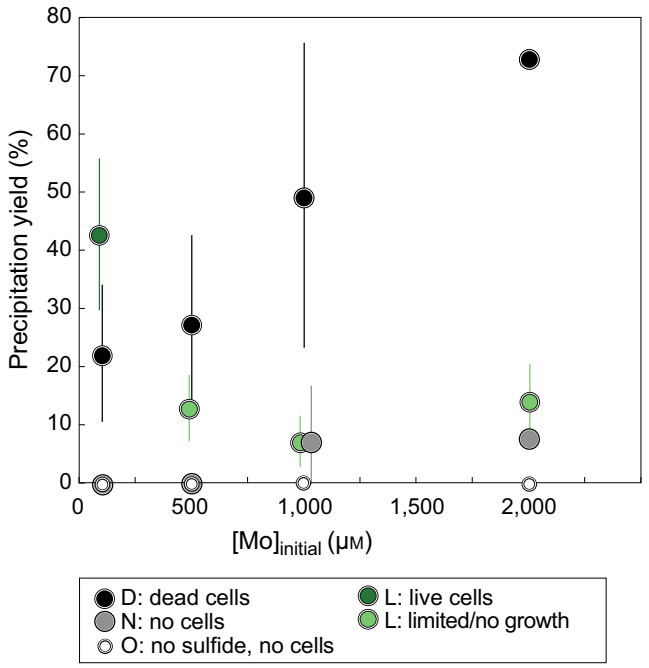

FIGURE 2 Molybdenum precipitation yields in aquatic sulfidic cultures. Mo precipitates in the presence of dead/lysed cells at high sulfide concentration (>1 mM, Figure S2) and not in cell-free control experiments. Tabulated data are shown in Table S1. Live cultures in 500 μM Mo experienced limited growth and therefore lower sulfide concentrations close to initial levels (0.32 mM) [Colour figure can be viewed at wileyonlinelibrary.com]

The high Mo levels in our experiments (~mM) compared to natural environments (~nM) would be a matter of concern if Mo-Mo self-complexation (e.g., Mo-dimers or Mo-trimers) acted as important intermediates in the Mo precipitation process. Polynuclear Mo sulfide species, including $Mo_2S_7^{2-}$, $Mo_4S_{15}^{6-}$, and $Mo_4S_{13}^{2-}$, have been reported from continuous acidification experiments with molar-level thiomolybdate solutions (Saxena, Jain, & Mittal, 1968). We can rule out this possibility from the low Mo precipitation yields (<10%) in N samples compared to ≤75% Mo precipitated in the D samples (Table S1). Also, the precipitation yields in D experiments scale linearly with Mo concentration (Figure 2) and not as a quadratic or cubic function of [Mo] as would be expected if Mo-dimers and Mo-trimers controlled the precipitation process, respectively. From these data, it is clear that the presence of dead and/or lysed cells at ~mM sulfide levels promotes Mo removal in the experiment. Moreover, our EXAFS and XANES results show that the Mo precipitates have molecular structures distinct from the starting material and similar to those found in natural euxinic sediments (as discussed below).

Potential Mo precipitation via solely microbiological processes was also investigated. *D. vulgaris* Hildenborough has an active Mo transport system similar to other bacteria involving a periplasmic binding protein (encoded on *modA*), a transmembrane permease lipoprotein (a product of *modB*), and a cytoplasmic ATP-binding protein (produced by *modC*) (Biswas et al., 2009; Grunden & Shanmugam, 1997). Several bacteria have an additional regulatory protein (*modE*) that prevents synthesis of the proteins for the molybdate transporter system under conditions where molybdate uptake exceeds enzymatic needs. Because this transporter system is inactive in heat-killed control experiments, Mo precipitation in our experiments cannot be associated with this process. Nevertheless, dead cells often have greater binding capacity than living ones presumably because cellular degradation increases the availability of functional groups capable of binding metals (Ferris, Fyfe, & Beveridge, 1988). Our result contrasts with previous observations on heat-killed cultures of *D. vulgaris* Hildenborough where only a small amount of Mo(VI) removal was observed (Tucker, Barton, & Thomson, 1997). Our experiments differ from previous ones mainly by the longer time available for reaction with dead cell material (42 days vs. 4 days). Also, sulfide concentrations were not measured directly in previous work and could

well have been lower than in our experiments, because bottles with sulfidic media were briefly opened after autoclaving and reflushed with H_2 or N_2 before heat-killed cells were added to the medium (Tucker et al., 1997). Hydrolysis of thiomolybdate species could occur and promote formation of molybdate at low sulfide concentrations (Erickson & Helz, 2000). In our study, the Hungate tubes with dead cells were kept closed at all times (also during autoclaving), and molybdate was carefully injected using a syringe and needle through the rubber septum into the anaerobic culture tube to minimize loss of ΣS(-II). Also, sulfide levels were high in all of our dead control experiments (ΣS(-II) = 1–13 mM, Figure S2). Therefore, we conclude that a combination of sufficient ΣS(-II), time available for reaction, and particulate organic matter (live or dead cell material) is essential to promote Mo precipitation.

3.3 | Molybdenum oxidation state and bonding environment when associated with particulate organic matter

The molecular structure of the Mo precipitates can provide new insight about the Mo burial pathways under sulfidic conditions. To determine the Mo oxidation state for our experimental samples, a three-point calibration curve was established using molybdenite, thiomolybdate, and the new synthetic Mo(V)-S compound, $(Ph_4P)_2[Mo_2S_8]$. The latter

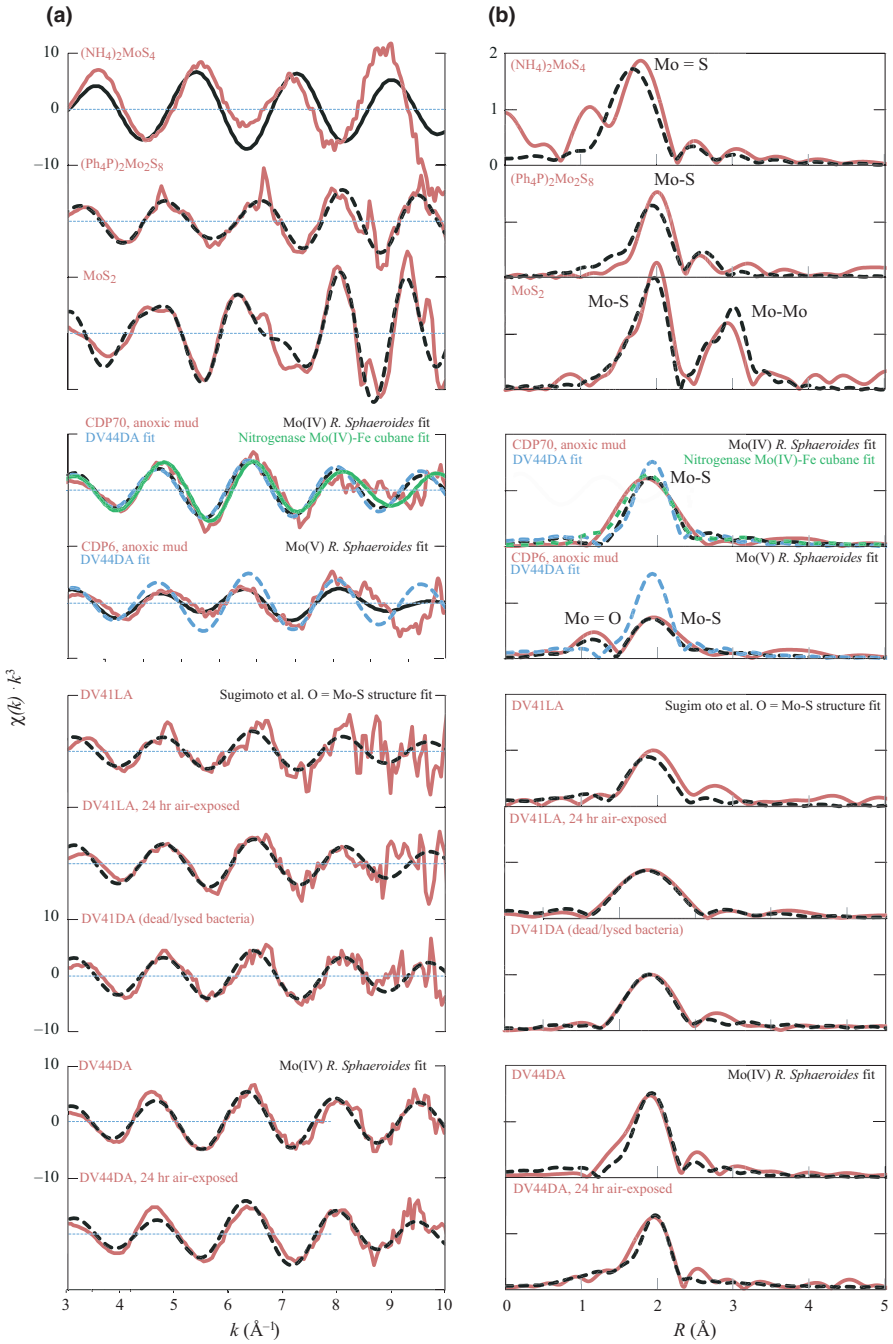

FIGURE 3 EXAFS spectra showing Mo-S reference compounds ($Mo^{IV}S_2$, $Mo^{V}_2S_8$, $Mo^{VI}S_4^{2-}$), two distinct anoxic mud sediments (CDP6, CDP70), and the spectra from cell-associated precipitates. The k^3-weighed spectra are shown (left column) with corresponding Fourier transform in R-space (right column). Dashed lines show our "best" fit, see text for details. The *x*-axis and *y*-axis are fixed in all panels [Colour figure can be viewed at wileyonlinelibrary.com]

TABLE 1 The modeled (guessed) structures are (a) molybdenite, MoS_2; (b) $[Ph_4P]_2[Mo^V_2S_8]$; (c) tetrathiomolybdate, MoS_4^{2-}; (e) reduced Moco enzyme, exemplified by DMSO Reductase from *R. Sphaeroides* with or without Mo-OH; (f) oxidized Moco enzyme, exemplified by sulfite oxidase at hi-pH (George et al., 1989), or structure g in Figure 4 (Sugimoto et al., 2008); (h) FeMo cofactor in nitrogenase. The coordination environments for a, b, c, e, f, g, and h are shown in Figure 4

Compound	Short name	Fitting model	R_k-factor	Fitting range	Mo-O			Mo-S			Sum bond valence V (Mo oxid. state)
				Å^{-1}	N	R (Å)	Σ^2 (Å^2)	N	R (Å)	Σ^2 (Å^2)	
Reference materials											
MoS_2		A	0.08	3.26–13.45				6	2.409 ± 0.016	0.006	3.7 (IV)
$[Ph_4P]_2[Mo^V_2S_8]$ with Ce(IV)	M4	B	0.191	2–10				1	2.108	0.020	5.0 (V)
								2	2.314	0.020	
								2	2.382	0.003	
MoS_4^{2-}		C	0.288	3–9				4	2.178 ± 0.028	0.005	6.0 (VI)
–	Alternative fit		0.029	3–12				4	2.211 ± 0.017	0.004 ± 0.002	5.5 (VI)
Mo_3O_8 - n H_2O			0.071	3–10	2	1.652 ± 0.066	0.003				5.5 (VI,V)
					2	1.826 ± 0.125	0.006 ± 0.006				
Samples											
Sulfate-reducing bacteria, heat-killed, 0.1 mM Mo	DV41DA	¥	0.144	3.65–8.58	1	1.73	0.013 ± 0.013	1	2.337	0.020	4.8 (V)
								1	2.361	0.020	
								1	2.397	0.007	
								1	2.406	0.003	
–	Alternative fit		0.110	3–9	1	1.688 ± 0.071	0.004 ± 0.010	4	2.350 ± 0.062	0.009 ± 0.011	5.2 (V)
Sulfate-reducing bacteria, heat-killed, 2 mM Mo	DV44DA	E	0.127	2.387–11	1	1.72	0.0043 ± 0.0043	2	2.40	0.020	4.0 (IV)
								2	2.45	0.0154 ± 0.0257	
–	Alternative fit		0.137	2.387–11	1	1.76	0.020	2	2.40	0.020	3.8 (IV)
								2	2.45	0.0138 ± 0.0219	
–	Alternative fit		0.097	3–10	0.5	1.658 ± 0.071	0.003	5	2.371 ± 0.035	0.009 ± 0.005	4.4 (IV)
Same as above, left in open air for 24 hrs	DV44DAox	E	0.150	3.457–13	1	1.72	0.020	2	2.40	0.0060 ± 0.0036	4.0 (IV)
								2	2.45	0.020	
–	Alternative fit		0.293	3.457–13	1	1.92	0.020	4	2.335	0.0067 ± 0.0054	4.0 (IV)
Sulfate-reducing bacteria, alive 0.1 mM Mo	DV41LA	¥	0.282	2.908–8.355	1	1.73	0.020	1	2.337	0.020	4.8 (V)
								1	2.361	0.020	
								1	2.390	0.007	
								1	2.406	0.003	
Same as above, left in open air for 24 hrs	DV41LAox	¥	0.090	3.607–8	1	1.73	0.0195 ± 0.0355	1	2.337	0.003	4.8 (V)
								1	2.361	0.020	
								2	2.400	0.0146 ± 0.0330	

continues

TABLE 1 (continued)

Compound	Short name	Fitting model	R_k-factor	Fitting range Å^{-1}	Mo-O N	Mo-O R (Å)	Mo-O Σ^2 (Å^2)	Mo-S N	Mo-S R (Å)	Mo-S Σ^2 (Å^2)	Sum bond valence V (Mo oxid. state)
Sediments											
Anoxic mud, Type Mo-S, Lake Cadagno	CDP70X	†	0.127	3–9	1	1.944	0.002	4	2.352	0.0096 ± 0.0106	4.2 (IV)
					1	2.144	0.0063				
-	Alternative fit E DMSO reductase		0.193	3–9	1	1.72	0.020	1	2.38	0.003	4.0 (IV)
								1	2.42	0.0075	
								2	2.45	0.015	
-	Alternative fit H Mo-Fe cubane		0.092	3–9				4	2.355	0.0032 ± 0.011	3.9 (IV)
								1	2.50	0.010	
Anoxic mud, Type Mo-OS Lake Cadagno	CDP6X	F	0.26	3–9	1	1.76	0.003	1	2.38	0.008	5.9 (VI)
								1	2.42	0.007	
								2	2.45	0.015	

displays a K-edge energy between that of Mo(IV)-S and Mo(VI)-S compounds, verifying the expected metal oxidation state (Figure 1, Figure S4). The microbial precipitates display a reduced Mo XANES signature distinctly lower than that of hexavalent thiomolybdate. In an (E_M-E_K) vs. E_K cross-plot (Figure 1), the microbial precipitate DV44DA (2 mM Mo, dead control) plots on the Mo-S array near Mo^{IV}-S compounds, yet distinctly above MoS_2, and together with modern anoxic sediments from Lake Cadagno (e.g., CDP70). Two microbial precipitates DV41LA and DV41DA (0.1 mM Mo, alive and dead control, respectively) also plot with the Mo-S compounds, but with distinctly higher oxidation state manifested by a K-edge between that of Mo^{V}-S and Mo^{VI}-S. Small pre-edge inflections, known as the "oxo-edge" feature, suggest that Mo=O bonds (or perhaps Mo=S) are present in all of the cell-associated precipitates.

The Mo bonding environment was further characterized using EXAFS. Figure 3 shows the Mo-K-edge EXAFS spectra, selected fits and the corresponding Fourier transforms of microbial precipitates, together with Mo-S reference materials and euxinic sediments from Lake Cadagno. The results of the curve fitting analyses are summarized in Table 1 (full details in supplement, Table S2). All the cell-associated precipitates fit the EXAFS equation with only 3–4 Mo-S ligands. Therefore, we conclude that both molybdenite (MoS_2) and MoS_3 with 5.3–6 Mo-S ligands are not the dominant phase precipitating in our experiments (Cramer, Liang, Jacobson, Chang, & Chianelli, 1984). This conclusion differs from previous conclusions, suggesting that MoS_2 is present based on an indirect characterization, that is, observation of curved layers in high resolution TEM images (Biswas et al., 2009).

Precipitate from a live microbial culture (DV41LA) shows an EXAFS signature that is indistinguishable from the dead control experiment (DV41DA), indicating that a similar Mo precipitation mechanism operates whether the cells are alive or dead. Modeling of EXAFS spectra suggests that these two precipitates from 0.1 mM Mo media (DV41LA and DV41DA) contain shorter Mo-S bonds, at 2.33–2.36Å, compared to the precipitate formed in 2.0 mM Mo media (DV44DA) with Mo-S bonds at 2.40–2.45 Å (Tables 1, S2). This result is perfectly consistent with the XANES evidence for a higher Mo oxidation state in the former (DV41LA and DV41DA) and predominantly reduced Mo(IV)-sulfide compounds in the latter (DV44DA) (Table 1). For both types of spectra, best EXAFS model fits contain 1-2 Mo-O at a short distance of 1.73–1.76Å indicative of terminal oxygen bonds (Mo=O). Again, this is in good agreement with the small, but significant, "oxo-edge" features visible as pre-edge inflections in the derivative XANES spectra. This oxo-edge feature becomes more prominent when Mo sits in a higher oxidation state and with more Mo=O bonds present (e.g., MoO_4^{2-}) (Dahl, Chappaz et al., 2013; Kutzler, Natoli, Misemer, Doniach, & Hodgson, 1980). Indeed, cell-associated precipitates with predominantly Mo^{V}-S and Mo^{VI}-S features show a more distinctive pre-edge inflection than those with predominantly Mo^{IV}-S features (Figure S4). Importantly, these small oxo-edge features are also observed in modern anoxic muds (Dahl, Chappaz et al., 2013) and in some Mo enzymes (e.g., George, Garrett, Prince, & Rajagopalan, 1996; George, Hilton, Temple, Prince, & Rajagopalan, 1999; George et al., 1989).

TABLE 2 Mo/Fe of the pellet fraction of dead cell cultures (D) separated from the solution by centrifugation after 42 days. No pellets were visible in the cell-free control experiments (O, N). Uncertainties represent analytical error (±2 *SD*)

Experiment	Mo µg	Fe µg	Mo/Fe[a] mol/mol
100 µM MoO_4^{2-}	5 ± 0[b]	3.1 ± 0.1[b]	0.9 ± 0.05[b]
500 µM MoO_4^{2-}	167 ± 1	4.2 ± 0.0	23 ± 0.2
1,000 µM MoO_4^{2-}	118 ± 1	4.5 ± 0.0	15.3 ± 0.1
2,000 µM MoO_4^{2-}	226 ± 1	1.7 ± 0.0	76.0 ± 1.6

[a]ICP-MS data.
[b]This pellet was harvested by NaOH.

As a quick test of sensitivity toward oxidation, both spectral types were also measured after 24 hr air exposure covered only by O_2-permeable Kapton® tape. No chemical change was evident in the XAFS spectra. Hence, the Mo compounds do not appear to be particularly air-sensitive.

3.4 | Non-Fe-dependent removal

Molybdenum and iron contents in the cell-associated precipitates are given in Table 2. The molar Mo/Fe ratios (0.9 to 76) in the precipitates are distinctly higher than those for $FeMo_{0.6}S_{2.8}$ (Mo/Fe = 0.6 ± 0.1), ruling out the possibility of $FeMo_{0.6}S_{2.8}$ as the precipitated phase. Also, the FeMo cofactor in nitrogenase contains too much iron (Mo/Fe = 0.06–0.17) to account for the majority of Mo in our samples (Madden, Krezel, Allen, Ludden, & Shah, 1992; Shah & Brill, 1977). This finding is particularly important, because it implies that Mo can be removed in the absence of iron. We propose that a ternary system is responsible for Mo removal: Mo—sulfide—particulate organic matter.

Even though the cell-associated precipitates are Fe-poor, ruling out $FeMo_{0.6}S_{2.8}$ and whole nitrogenase enzymes, the structure of the Mo coordination environment (say, within 3Å) may still resemble that observed in most other Mo enzymes, where Fe is not part of the immediate bonding environment. This is relevant for the OM removal pathways, to be discussed below.

3.5 | Similarities to Mo enzymes

Our EXAFS, XANES, and ICP-MS results demonstrate that the cell-associated Mo precipitates are different from any of the starting materials (e.g., molybdate and thiomolybdates) and Mo compounds that have previously been discussed (including MoS_2, $FeMo_{0.6}S_{2.8}$, and nitrogenase). Rather, our EXAFS and XANES data show that the molecular structures around Mo in the cell-associated precipitates share many attributes with those found in Mo enzymes, where Fe is not present in the immediate coordination environment (summarized Table S3).

With the exception of bacterial nitrogenase, where Mo is found in the FeMo cofactor (Fay, 1992), Mo is bound to a pterin forming the molybdenum cofactor (Moco), which is the active compound at the catalytic site of all other molybdenum enzymes (Mendel & Bittner, 2006).

Moco enzymes are categorized into three families (Hille, 1996): (i) the xanthine oxidase family (e.g., aldehyde oxidoreductase), (ii) sulfite reductase and assimilatory nitrate reduction family, and (iii) the dimethylsulfoxide (DMSO) reductase family (e.g., dissimilatory nitrate reductase). In all three enzyme families, Mo is coordinated to one or two pterin ligands, each of which are bridged via two Mo-S ligands (Figure 4).

The EXAFS spectra associated with the reduced Mo(IV)-S compounds (DV44DA and DV44DAox) and associated with dead sulfate-reducing bacteria and Moco in DMSO reductase from *Rhodobacter Sphaeroides* (George et al., 1999) display similar coordination geometry (Figure 4e; Tables S2 and S3). This enzyme belongs to the same family as dissimilatory nitrate reductase, which is found in the periplasm of a related strain of *Desulfovibrio* (*D. desulfuricans* ATCC 27774; Moura, Gonzalez, Moura, and Fauque (2007)). This means the immediate coordination environment around each Mo atom (Mo-O, Mo-S) is similar to those observed in the enzyme. Unfortunately, our EXAFS data do not constrain the type of atoms beyond ~2.6Å (i.e., one can fit Mo-C at the expected distances, but it does not significantly improve the fit to the EXAFS spectra). In fact, cell-associated precipitates display EXAFS spectra that also fit with the coordination environment in nitrogenase (Figure 3), where Mo-Fe distance is ~2.8Å (Cramer, Hodgson, Gillum, & Mortenson, 1978). Nevertheless, Fe is also not required to fit the structural models, and the low Fe/Mo ratio in the precipitates rules out nitrogenase as dominant Mo compound in our samples. The "humic substance" used to precipitate Mo from sulfidic solutions in Helz et al. (1996) and provided by Aldrich at that time was not purified for Fe and Mn oxides that are present at significant levels in natural organic matter. Therefore, the EXAFS model fits may include Fe, but this result is not representative of Mo-particulate OM interactions, unlike our study that produced Fe-depleted particulate OM from dead SRB.

The cell-associated precipitates with shorter Mo-S bonds and Mo in a higher average oxidation state (Figure 1, DV41LA, DV41DA, DV41LAox) also fit with previous characterizations of Moco enzymes, when Mo sits in the +V/+VI oxidation state (Moura et al., 2007). Broadly speaking, Mo sits in a similar coordination environment in all Moco compounds, regardless of Mo oxidation state (Table S3). Therefore, our EXAFS and XANES data are consistent and suggest Mo can be present as +IV and +V (perhaps even in +VI) state on the cell material from dead sulfate-reducing bacteria. Molybdenum enzymes are found in various strains of *Desulfovibrio*, including dissimilatory nitrate reductase (*D. desulfuricans* ATCC 27774; Moura et al. (2007)), aldehyde oxidoreductase (*D. gigas;* Romão et al. (1995), *D. desulfuricans;* Rebelo et al. (2000)), Mo-Fe-S proteins of unknown physiological activity (*D. africanus;* Hatchikian and Bruschi (1979)), and nitrogenase in *D. vulgaris* Hildenborough (Postgate & Kent, 1985). However, there is no reason to believe that all the Mo in the cell-associated precipitates is hosted in entire enzymes, only that similar Mo compounds are present; for example, synthetic (abiotic) Mo(V)-sulfide compounds with two polysulfide rings and a Mo=O bond (Figure 4g) offer an

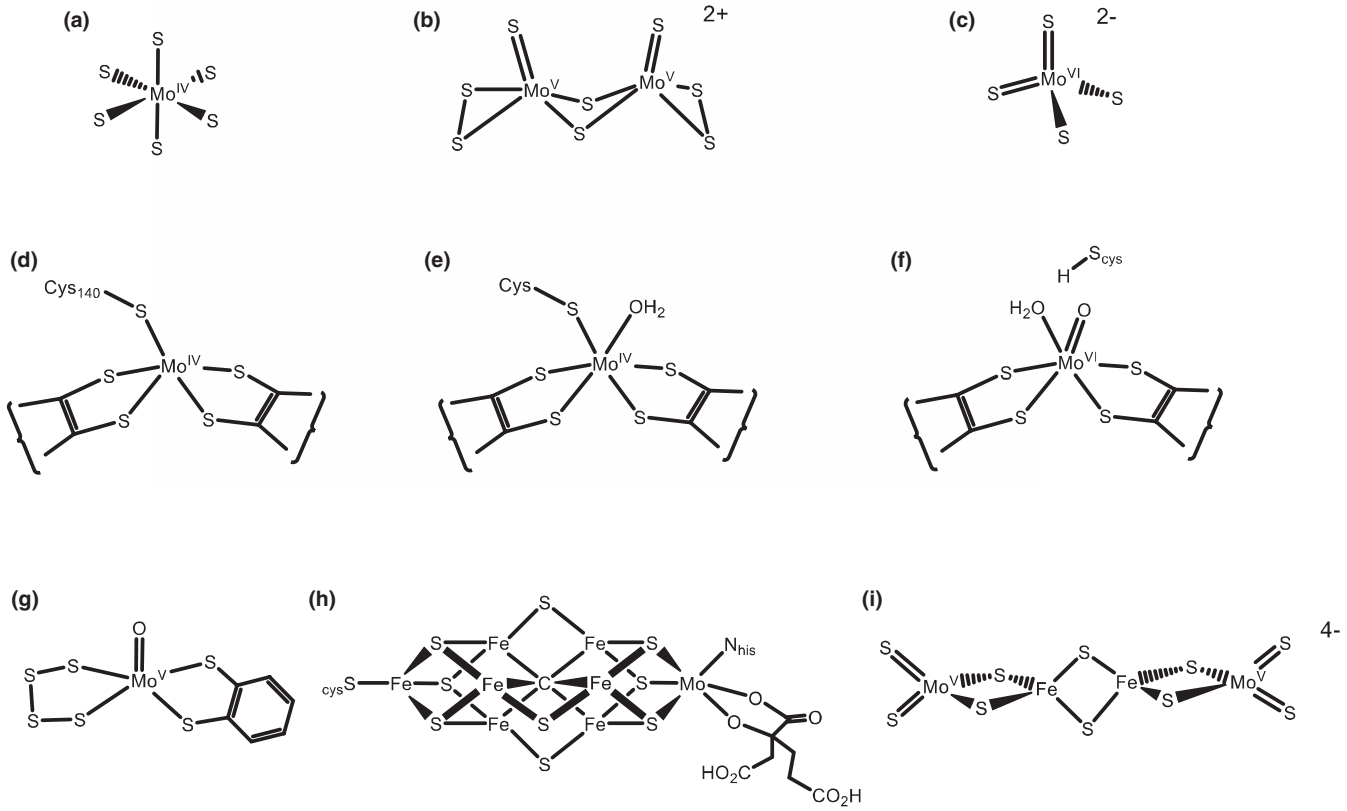

FIGURE 4 Molybdenum coordination environment in some relevant compounds. (a) molybdenite, Mo(IV)S_2, a hexagonal mineral (Dickinson & Pauling, 1923). (b) A molybdenum(V)-S dimer previously described by Pan et al. and synthesized in this study for comparison (Pan et al., 1984). (c) Tetrahedral coordination of the tetrathiomolybdate anion, MoS_4^{2-}. In biology, the Mo-cofactor in all (~30), but one class (nitrogenase) enzymes, shows the same four basal Mo-S ligands (e.g., pterin side chains) and various ligands at the pole depending on redox state (Mo=O, Mo-OH and Mo-S). Proposed structures are shown for (d) nitrate reductase in its reduced state (Pan et al., 1984). (e) DMSO reductase in its reduced state (Dias, 1999). (f) DMSO reductase in its oxidized state (George et al., 1999; Mcalpine, Mcewan, Shaw, & Bailey, 1997), respectively. (g) A synthetic Mo-S compound with similar coordination environment, but coordinated by two polysulfide rings (George et al., 1999; Mcalpine et al., 1997). (h) Cuboid Fe-Mo-S cluster resembling the proposed structure of the FeMo cofactor in nitrogenase (Sugimoto et al., 2008). (i) Linear complex consisting of a 2 Fe-2Mo cluster coordinated to MoS_4^{2-}, thought relevant for FeS assisted Mo removal in nature (Cramer et al., 1978; Helz et al., 2014; Venters et al., 1986)

alternative match to the cell-associated Mo(V)-sulfides. On the other hand, we can speculate that the passive synthesis of these Moco-like compounds in the vicinity of (heat-killed/lysed) cell material is important precursors in the synthesis of Mo enzymes among cells in sulfidic aqueous environments. Perhaps, these compounds are even catalyzing redox reactions (e.g., O-atom transfer reactions) for early life to adopt, before Mo enzymes became genetically coded.

3.6 | The particulate organic matter pathway: Implications for molybdenum cycling in marine sulfidic systems and implications for the Mo–TOC redox proxy

The EXAFS and XANES spectra of cell-associated precipitates compare rather well with the spectra observed in euxinic muds from Lake Cadagno (CDP70, Figure 1 and 3), suggesting a Mo-OM pathway could be responsible for euxinic Mo removal in some natural sulfidic systems. At the molecular level, the FeMo cubane structure in nitrogenase and the Moco enzymes show quite similar EXAFS spectra (Figure 3). Therefore, both structures are viable models for the euxinic sediments. Here, the MoFe-cubane gives a slightly better fit (lower R_k-factor; 0.092 vs. 0.127; Table 1; Table S2), pointing in the direction that Mo might also take the Fe pathway in Lake Cadagno. Nevertheless, we cannot exclude any of these pathways.

Among the potential mechanisms responsible for Mo burial under sulfidic conditions, the Fe pathway has been favored mostly because of the experimental work done with Fe (Bostick et al., 2003; Freund et al., 2016; Helz et al., 2004, 2011) that identified the reactions involved when Mo co-precipitates with Fe sulfide and from observations that dissolved Mo concentrations in euxinic lake settings become constant below depths where sulfidic waters become saturated with iron monosulfide (Helz et al., 2011). However, Mo also precipitates with dead/lysed cells and with Fe-contaminated humic acids in sulfidic solution (Helz et al., 1996), and the constant, nonzero dissolved Mo profile may also arise from the presence of Mo on non-sinking

organic material (e.g., colloidal, and small particulate organic matter, e.g., <0.2 μm). This is expected, as a large portion of (non-sinking) Mo in the sulfidic waters sits in the filterable fraction (>0.2 μm) (Dahl, Anbar et al., 2010). Mo–OM association occurring within the water column has been suggested based on correlations in sediments and characterizations of geological samples (e.g., Lyons et al., 2009 and references therein). However, previous experimental work with particulate OM and thiomolybdates has not satisfactorily demonstrated that this could be an independent pathway. Our new results fill this gap and clearly demonstrate that under sulfidic conditions dissolved Mo(VI) can be adsorbed and reduced at the surface of particulate organic matter, represented by dead/lysed SRB.

We conclude that the cell-associated Mo precipitates are structurally similar to that observed in anoxic muds and black shales (i.e., sedimentary rocks with ~100 ppm Mo). Based on these new observations, we propose that Mo scavenging in anoxic and sulfidic environments can occur with particulate OM and that the Mo-TOC relationship observed in the sediments can reflect a direct interaction between Mo and particulate OM (e.g., dead/lysed *D. vulgaris* Hildenborough). Our new results are consistent with a pathway for Mo removal that minimizes the involvement of Fe. This organic removal pathway may be unique relative to iron-dependent removal pathway(s), and these pathways therefore might operate in parallel and/or in conjunction depending on the environmental conditions (Algeo & Lyons, 2006; Dahl, Anbar et al., 2010; Helz et al., 1996).

ACKNOWLEDGMENTS

Heidi Grøn Jensen (SDU) and Peter Søholt (SDU) assisted in the laboratory. Thanks to Steve Romaniello and Moutusi Roy from Arizona State University for fruitful discussions and ICPMS concentration analyses of a complementary set of microbial precipitates (not reported here). Funding was provided from Nordic Center for Earth Evolution (NordCEE) of the Danish National Research Foundation (Danmarks Grundforskningsfond, grant number DNRF53) T.W.D. was sponsored from the VILLUM Foundation (ID: 1168439 and VKR023127). ACS-PRF 54583-DNI2 and NSF-EAR 1503596 provided funding for AC.

REFERENCES

Algeo, T. J., & Lyons, T. W. (2006). Mo–total organic carbon covariation in modern anoxic marine environments: Implications for analysis of paleoredox and paleohydrographic conditions. *Paleoceanography*, *21*, 1–23.

Algeo, T. J., & Tribovillard, N. (2009). Environmental analysis of paleoceanographic systems based on molybdenum–uranium covariation. *Chemical Geology*, *268*, 211–225.

Allen, F. H. (2002). The Cambridge Structural Database: A quarter of a million crystal structures and rising. *Acta Crystallographica Section B: Structural Science*, *58*, 380–388.

Altermatt, D., & Brown, I. D. (1985). The automatic searching for chemical bonds in inorganic crystal structures. *Acta Crystallographica Section B: Structural Crystallography and Crystal Chemistry*, *B41*, 240–244.

Amrhein, C., Mosher, P. A., & Brown, A. D. (1993). The effects of redox on Mo, U, B, V, and As solubility in evaporation pond soils. *Soil Science*, *155*, 249–255.

Anbar, A. D., & Knoll, A. H. (2002). Proterozoic ocean chemistry and evolution: A bioinorganic bridge? *Science*, *297*, 1137–1142.

Ardakani, O. H., Chappaz, A., Sanei, H., & Mayer, B. (2016). Effect of thermal maturity on remobilization of molybdenum in black shales. *Earth and Planetary Science Letters*, *449*, 311–320.

Arnold, G. L., Anbar, A. D., Barling, J., & Lyons, T. W. (2004). Molybdenum isotope evidence for widespread anoxia in mid-proterozoic oceans. *Science*, *304*, 87–90.

Bertine, K. (1972). The deposition of molybdenum in anoxic waters. *Marine Chemistry*, *1*, 43–53.

Biswas, K. C., Woodards, N. A., Xu, H., & Barton, L. L. (2009). Reduction of molybdate by sulfate-reducing bacteria. *BioMetals*, *22*, 131–139.

Bostick, B. C., Fendorf, S., & Helz, G. R. (2003). Differential adsorption of molybdate and tetrathiomolybdate on pyrite (FeS2). *Environmental Science and Technology*, *37*, 285–291.

Brown, I. D., & Altermatt, D. (1985). Bond-valence parameters obtained from a systematic analysis of the inorganic crystal structure database. *Acta Crystallographica Section B: Structural Crystallography and Crystal Chemistry*, *B41*, 244–247.

Chappaz, A., Gobeil, C., & Tessier, A. (2008). Geochemical and anthropogenic enrichments of Mo in sediments from perennially oxic and seasonally anoxic lakes in Eastern Canada. *Geochimica et Cosmochimica Acta*, *72*, 170–184.

Chappaz, A., Lyons, T. W., Gregory, D. D., Reinhard, C. T., Gill, B. C., Li, C., & Large, R. R. (2014). Does pyrite act as an important host for molybdenum in modern and ancient euxinic environments? *Geochimica et Cosmochimica Acta*, *126*, 112–122.

Chen, G., Ford, T., & Clayton, C. (1998). Interaction of sulfate-reducing bacteria with molybdenum dissolved from sputter-deposited molybdenum thin films and pure molybdenum powder. *Journal of Colloid and Interface Science*, *204*, 237–246.

Cline, J. D. (1969). Spectrophotometric determination of hydrogen sulfide in natural waters. *Limnology and Oceanography*, *14*, 454.

Cramer, S. P., Hodgson, K. O., Gillum, W. O., & Mortenson, L. E. (1978). The molybdenum site of nitrogenase. Preliminary structural evidence from X-Ray absorption spectroscopy. *Journal of the American Chemical Society*, *100*, 3398–3407.

Cramer, S. P., Liang, K. S., Jacobson, A. J., Chang, C. H., & Chianelli, R. R. (1984). EXAFS studies of amorphous molybdenum and tungsten trisulfides and triselenides. *Inorganic Chemistry*, *23*, 1216–1221.

Crusius, J., Calvert, S., Pedersen, T., & Sage, D. (1996). Rhenium and molybdenum enrichments in sediments as indicators of oxic, suboxic and sulfidic conditions of deposition. *Earth and Planetary Science Letters*, *145*, 65–78.

Dahl, T. W., Anbar, A. D., Gordon, G. W., Rosing, M. T., Frei, R., & Canfield, D. E. (2010). The behavior of molybdenum and its isotopes across the chemocline and in the sediments of sulfidic Lake Cadagno, Switzerland. *Geochimica et Cosmochimica Acta*, *74*, 144–163.

Dahl, T. W., Chappaz, A., Fitts, J. P., & Lyons, T. W. (2013). Molybdenum reduction in a sulfidic lake: Evidence from X-ray absorption fine-structure spectroscopy and implications for the Mo paleoproxy. *Geochimica et Cosmochimica Acta*, *103*, 213–231.

Dahl, T. W., Hammarlund, E. U., Anbar, A. D., Bond, D. P. G., Gill, B. C., Gordon, G. W., … Canfield, D. E. (2010). Devonian rise in atmospheric oxygen correlated to the radiations of terrestrial plants and large predatory fish. *Proceedings of the National Academy of Sciences*, *107*, 17911–17915.

Dahl, T. W., Ruhl, M., Hammarlund, E. U., Canfield, D. E., Rosing, M. T., & Bjerrum, C. J. (2013). Tracing euxinia by molybdenum concentrations in sediments using handheld x-ray fluorescence spectroscopy (HH-XRF). *Chemical Geology*, *360–361*, 241–251.

Dias (1999) Crystal structure of the first dissimilatory nitrate reductase at 1.9 Å solved by MAD methods. *Structure*, *7*, 65–79.

Dickinson, R. G., & Pauling, L. (1923). The crystal structure of molybdenite. *Journal of the American Chemical Society*, *45*, 1466–1471.

Erickson, B. E., & Helz, G. R. (2000). Molybdenum(VI) speciation in sulfidic waters: Stability and lability of thiomolybdates. *Geochimica et Cosmochimica Acta*, *64*, 1149–1158.

Fay, P. (1992). Oxygen relations of nitrogen fixation in cyanobacteria. *Microbiology and Molecular Biology Reviews*, *56*, 340–373.

Ferris, F. G., Fyfe, W. S., & Beveridge, T. J. (1988). Metallic ion binding by bacillus subtilis – implications for the fossilization of microorganisms. *Geology*, *16*, 149–152.

Freund, C., Wishard, A., Brenner, R., Sobel, M., Mizelle, J., Kim, A., … Morford, J. L. (2016). The effect of a thiol-containing organic molecule on molybdenum adsorption onto pyrite. *Geochimica et Cosmochimica Acta*, *174*, 222–235.

George, G. N., Garrett, R. M., Prince, R. C., & Rajagopalan, K. (1996). The molybdenum site of sulfite oxidase: A comparison of wild-type and the cysteine 207 to serine mutant using x-ray absorption spectroscopy. *Journal of the American Chemical Society*, *118*, 8588–8592.

George, G. N., Hilton, J., Temple, C., Prince, R. C., & Rajagopalan, K. V. (1999). Structure of the molybdenum site of dimethyl sulfoxide reductase. *Journal of the American Chemical Society*, *121*, 1256–1266.

George, G., Kipke, C., Prince, R., Sunde, R., Enemark, J., & Cramer, S. (1989). Structure of the active site of sulfite oxidase. X-ray absorption spectroscopy of the Mo (IV), Mo (V), and Mo (VI) oxidation states. *Biochemistry;(USA)*, *28*, 5075–5080.

Glass, J. B., Chappaz, A., Eustis, B., Heyvaert, A. C., Waetjen, D. P., Hartnett, H. E., & Anbar, A. D. (2013). Molybdenum geochemistry in a seasonally dysoxic Mo-limited lacustrine ecosystem. *Geochimica et Cosmochimica Acta*, *114*, 204–219.

Grunden, A. G., & Shanmugam, K. T. (1997). Molybdate transport and regulation in bacteria. *Archives of Microbiology*, *18*, 345–354.

Hatchikian, E. C., & Bruschi, M. (1979). Isolation and characterization of a molybdenum iron-sulfur protein from Desulfovibrio Africanus. *Biochemical and Biophysical Research Communications*, *86*, 725–734.

Helz, G. R., Bura-Nakić, E., Mikac, N., & Ciglenečki, I. (2011). New model for molybdenum behavior in euxinic waters. *Chemical Geology*, *284*, 323–332.

Helz, G., Erickson, B. E., & Vorlicek, T. P. (2014). Stabilities of thiomolybdate complexes of iron; Implications for retention of essential trace elements (Fe, Cu, Mo) in sulfidic waters. *Metallomics*, *6*, 1131–1140.

Helz, G. R., Miller, C. V., Charnock, J. M., Mosselmans, J. F. W., Pattrick, R., Garner, C. D., & Vaughan, D. J. (1996). Mechanism of molybdenum removal from the sea and its concentration in black shales: EXAFS evidence. *Geochimica et Cosmochimica Acta*, *60*, 3631–3642.

Helz, G. R., Vorlicek, T. P., & Kahn, M. D. (2004). Molybdenum Scavenging by Iron Monosulfide. *Environmental Science and Technology*, *38*, 4263–4268.

Hille, R. (1996). The mononuclear molybdenum enzymes. *Chemical Reviews*, *96*, 2757–2816.

Kutzler, F. W., Natoli, C., Misemer, D., Doniach, S., & Hodgson, K. O. (1980). Use of one electron theory for the interpretation of near edge structure in K shell x ray absorption spectra of transition metal complexes. *The Journal of Chemical Physics*, *73*, 3274.

Lapasset, J., Chezau, N., & Belougne, P. (1976). Nouvel affinement de la structure cristalline du thiomolybdate d'ammonium. *Acta Crystallographica Section B: Structural Crystallography and Crystal Chemistry*, *32*, 3087–3088.

Lyons, T. W., Anbar, A. D., Severmann, S., Scott, C., & Gill, B. C. (2009). Tracking euxinia in the ancient ocean: A multiproxy perspective and proterozoic case study. *Annual Review of Earth and Planetary Sciences*, *37*, 507–534.

Madden, M. S., Krezel, A. M., Allen, R. M., Ludden, P. W., & Shah, V. K. (1992). Plausible structure of the iron-molybdenum cofactor of nitrogenase. *Proceedings of the National Academy of Sciences*, *89*, 6487.

Mcalpine, A., Mcewan, A. G., Shaw, A., & Bailey, S. (1997). Molybdenum active centre of DMSO reductase from Rhodobacter capsulatus: Crystal structure of the oxidised enzyme at 1.82-Å resolution and the dithionite-reduced enzyme at 2.8-Å resolution. *Journal of Biological Inorganic Chemistry : JBIC : A Publication of the Society of Biological Inorganic Chemistry*, *2*, 690–701.

Mendel, R. R., & Bittner, F. (2006). Cell biology of molybdenum. *Biochimica et Biophysica Acta*, *1763*, 621–635.

Migneault, I., Dartiguenave, C., Bertrand, M. J., & Waldron, K. C. (2004). Glutaraldehyde: Behavior in aqueous solution, reaction with proteins, and application to enzyme crosslinking. *BioTechniques*, *37*, 790–802.

Moura, J. J. G., Gonzalez, P., Moura, I., & Fauque, G. (2007) *Dissimilatory nitrate and nitrite ammonification by sulphate-reducing eubacteria*. 241–264: Cambridge University Press.

Nameroff, T. J., Balistrieri, L. S., & Murray, J. W. (2002). Suboxic trace metal geochemistry in the Eastern Tropical North Pacific. *Geochimica et Cosmochimica Acta*, *66*, 1139–1158.

Pan, W.-H., Harmer, M. A., Halbert, T. R., & Stiefel, E. I. (1984). Induced internal redox processes in molybdenum-sulfur chemistry: Conversion of MoS4- to Mo2S82- by organic disulfides. *Journal of the American Chemical Society*, *106*, 459–460.

Postgate, J. R., & Kent, H. M. (1985). Diazotrophy within desulfovibrio. *Journal of General Microbiology*, *131*, 2119–2122.

Poulson Brucker, R. L., Mcmanus, J., Severmann, S., & Berelson, W. M. (2009). Molybdenum behavior during early diagenesis: Insights from Mo isotopes. *Geochemistry Geophysics Geosystems*, *10*, 1–25.

Rebelo, J., Macieira, S., Dias, J. M., Huber, R., Ascenso, C. S., Rusnak, F., … Romáo, M. J. (2000). Gene sequence and crystal structure of the aldehyde oxidoreductase from Desulfovibrio desulfuricans ATCC 27774. *Journal of Molecular Biology*, *297*, 135–146.

Romão, M. J., Archer, M., Moura, I., Moura, J. J. G., Legall, J., Engh, R., … Huber, R. (1995). Crystal structure of the xanthine oxidase-related aldehyde oxido-reductase from *D. gigas*. *Science*, *270*, 1170–1176.

Saxena, R. S., Jain, M. C., & Mittal, M. L. (1968). Electrometric investigations of an acid-thiomolybdate system and the formation of polyanions. *Australian Journal of Chemistry*, *21*, 91–96.

Scott, C., & Lyons, T. W. (2012). Contrasting molybdenum cycling and isotopic properties in euxinic versus non-euxinic sediments and sedimentary rocks: Refining the paleoproxies. *Chemical Geology*, *324–325*, 19–27.

Scott, C., Lyons, T. W., Bekker, A., Shen, Y., Poulton, S. W., Chu, X., & Anbar, A. D. (2008). Tracing the stepwise oxygenation of the Proterozoic ocean. *Nature*, *452*, 456–459.

Shah, V. K., & Brill, W. J. (1977). Isolation of an iron-molybdenum cofactor from nitrogenase. *Proceedings of the National Academy of Sciences of the United States of America*, *74*, 3249–3253.

Siebert, C., Nägler, T. F., Von Blanckenburg, F., & Kramers, J. D. (2003). Molybdenum isotope records as a potential new proxy for paleoceanography. *Earth and Planetary Science Letters*, *211*, 159–171.

Sugimoto, H., Suyama, K., Sugimoto, K., Miyake, H., Takahashi, I., Hirota, S., & Itoh, S. (2008). A new class of sulfido/oxo(dithiolene)-molybdenum(IV) complexes derived from sulfido/oxo-bis(tetrasulfido)molybdenum(IV) anions. *Inorganic Chemistry*, *47*, 10150–10157.

Taylor, S. R., & Mclennan, S. M. (1995). The geochemical evolution of the continental crust. *Reviews of Geophysics*, *33*, 241–265.

Tribovillard, N., Hatem, E., Averbuch, O., Barbecot, F., Bout-Roumazeilles, V., & Trentesaux, A. (2015). Iron availability as a dominant control on the primary composition and diagenetic overprint of organic-matter-rich rocks. *Chemical Geology*, *401*, 67–82.

Tribovillard, N., Riboulleau, A., Lyons, T., & Baudin, F. (2004). Enhanced trapping of molybdenum by sulfurized marine organic matter of marine origin in Mesozoic limestones and shales. *Chemical Geology*, *213*, 385–401.

Tucker, M. D., Barton, L. L., & Thomson, B. M. (1997). Reduction and immobilization of molybdenum by desulfovibrio desulfuricans. *Journal of Environmental Quality*, *26*, 1146–1152.

Tucker, M. D., Barton, L. L., & Thomson, B. M. (1998a). Reduction of Cr, Mo, Se and U by Desulfovibrio desulfuricans immobilized in polyacrylamide gels. *Journal of Industrial Microbiology & Biotechnology*, *20*, 13–19.

Tucker, M. D., Barton, L. L., & Thomson, B. M. (1998b). Removal of U and Mo from water by immobilized Desulfovibrio desulfuricans in column reactors. *Biotechnology and Bioengineering*, *60*, 88–96.

Tuit, C., Waterbury, J., & Ravizza, G. (2004). Diel variation of molybdenum and iron in marine diazotrophic cyanobacteria. *Limnology and Oceanography*, *49*, 978–990.

Venters, R. A., Nelson, M. J., Mclean, P. A., True, A. E., Levy, M. A., Hoffman, B. M., & Orme-Johnson, W. H. (1986). ENDOR of the resting state of nitrogenase molybdenum-iron proteins from Azotobacter vinelandii, Klebsiella pneumoniae, and Clostridium pasteurianum. Proton, iron-57, molybdenum-95, and sulfur-33 studies. *Journal of the American Chemical Society*, *108*, 3487–3498.

Vorlicek, T. P., & Helz, G. R. (2002). Catalysis by mineral surfaces: Implications for Mo geochemistry in anoxic environments. *Geochimica et Cosmochimica Acta*, *66*, 3679–3692.

Vorlicek, T. P., Kahn, M. D., Kasuya, Y., & Helz, G. R. (2004). Capture of molybdenum in pyrite-forming sediments: Role of ligand-induced reduction by polysulfides. *Geochimica et Cosmochimica Acta*, *68*, 547–556.

Widdel, F., & Bak, F. (1992). Gram-Negative Mesophilic Sulfate-Reducing Bacteria. In A. Balows, H. G. Trüper, M. Dworkin, W. Harder, & K.-H. Schleifer (Eds.), *The Prokaryotes: A Handbook on the Biology of Bacteria: Ecophysiology, Isolation, Identification, Applications* (pp. 3352–3378). New York, NY: Springer New York.

Wille, M., Kramers, J. D., Nägler, T. F., Beukes, N. J., Schröder, S., Meisel, T., … Voegelin, A. R. (2007). Evidence for a gradual rise of oxygen between 2.6 and 2.5 Ga from Mo isotopes and Re-PGE signatures in shales. *Geochimica et Cosmochimica Acta*, *71*, 2417–2435.

Xu, N., Christodoulatos, C., & Braida, W. (2006). Adsorption of molybdate and tetrathiomolybdate onto pyrite and goethite: Effect of pH and competitive anions. *Chemosphere*, *62*, 1726–1735.

SUPPORTING INFORMATION

Additional Supporting Information may be found online in the supporting information tab for this article.